Journal of Power Sources 352 (2017) 111–117

Contents lists available at ScienceDirect

Journal of Power Sources

journal homepage: www.elsevier.com/locate/jpowsour

Effectively suppressing vanadium permeation in vanadium redox flow battery application with modified Nafion membrane with nacre-like nanoarchitectures

Lesi Zhang, Ling Ling, Min Xiao, Dongmei Han, Shuanjin Wang**, Yuezhong Meng*

State Key Laboratory of Optoelectronic Materials and Technologies/The Key Laboratory of Low-carbon Chemistry & Energy Conservation of Guangdong Province, School of Materials Science and Engineering, Sun Yat-sen University, Guangzhou 510275, PR China

HIGHLIGHTS

- Nafion-$[PDDA/ZrP]_n$ with nacre-like nanostructures was fabricated by LbL method.
- The lamellar structure and Donnan exclusion suppress vanadium ion permeability.
- Nafion-$[PDDA/ZrP]_3$ exhibits higher performance in VRFB than pristine Nafion.

GRAPHICAL ABSTRACT

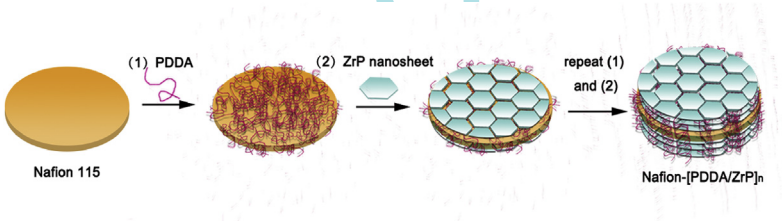

ARTICLE INFO

Article history:
Received 8 February 2017
Received in revised form
24 March 2017
Accepted 26 March 2017

Keywords:
Nacre-like nanostructure
Layer-by-layer self-assembly
Vanadium redox flow battery

ABSTRACT

A novel self-assembled composite membrane, Nafion-$[PDDA/ZrP]_n$ with nacre-like nanostructures was successfully fabricated by a layer-by-layer (LbL) method and used as proton exchange membrane for vanadium redox flow battery applications. Poly(diallyldimethylammonium chloride) (PDDA) with positive charges and zirconium phosphate (ZrP) nanosheets with negative charges can form ultra-thin nacre-like nanostructure on the surface of Nafion membrane via the ionic crosslinking of tightly folded macromolecules. The lamellar structure of ZrP nanosheets and Donnan exclusion effect of PDDA can greatly decrease the vanadium ion permeability and improve the selectivity of proton conductivity. The fabricated Nafion-$[PDDA/ZrP]_4$ membrane shows two orders of magnitude lower vanadium ion permeability (1.05×10^{-6} cm^2 min^{-1}) and 12 times higher ion selectivity than those of pristine Nafion membrane at room temperature. Consequently, the performance of vanadium redox flow batteries (VRFBs) assembled with Nafion-$[PDDA/ZrP]_3$ membrane achieved a highly coulombic efficiency (CE) and energy efficiency (EE) together with a very slow self-discharge rate. When comparing with pristine Nafion VRFB, the CE and EE values of Nafion-$[PDDA/ZrP]_3$ VRFB are 10% and 7% higher at 30 mA cm^{-2}, respectively.

1. Introduction

As one kind of energy storage systems, VRFBs have many advantages regarding high energy efficiency, moderate operating temperature, low environmental impact, large scale, and excellent cycle life, receiving wide attention in electrochemical energy storage. It is suitable for integrating electricity from various renewable energy sources into the grids [1–3]. VRFB is involving the same

* Corresponding author.
** Corresponding author.
E-mail addresses: wangshj@mail.sysu.edu.cn (S. Wang), mengyzh@mail.sysu.edu.cn (Y. Meng).

http://dx.doi.org/10.1016/j.jpowsour.2017.03.124
0378-7753/

metal in both half-cells, two pumps, and a battery stack section. The positive half-cell of which generally equipped with the electrolyte of V(IV)/V(V) redox couple whereas the negative half-cell is using the electrolyte of V(II)/V(III) redox couple in sulfuric acid solution. The electrolytes are separated by an ion exchange membrane (IEM) while the reactants contained in separate storage tanks. The electrolytes are recirculated through the redox flow cells where the electrochemical reactions (reduction and oxidation) take place [4,5].

As the key materials of VRFB, the ideal IEMs for VRFBs should possess low vanadium ion permeability, high proton conductivity, and good chemical stability. So far, commercial ion-exchange membranes such as Nafion perform high proton conductivity, good chemical and thermal stability. However, Nafion membranes encounter the problem of high vanadium ion cross-over which gives rise to high self-discharge rates and low EE [6]. There have been extensive research activities in the modification of Nafion-based membrane to reduce its vanadium ion permeability, for example, recasting with inorganic nanoparticles [7,8], impregnating porous membrane with Nafion solution [9], and in situ sol–gel reaction to incorporate inorganic oxide nanoparticles within the polar clusters of Nafion [10]. All of the aforementioned modification methods can be used to suppress the cross-over of vanadium ions through Nafion membranes, and in general improved the cell performance of VRFB.

Layered metal phosphate hydrate (LMPs) such as $Zr(HPO_4)_2 \cdot nH_2O$ (ZrP), $Ti(HPO_4)_2 \cdot nH_2O$, are known to show relatively high proton conductivity and much higher ion exchange capacity. Protons can move through the hydrogen-bond networks between interlayer water molecules and -HPO_4 groups in LMPs [11]. α-ZrP can be easily synthesized and fully exfoliated into individual layers and uniformly dispersed in the water [12]. The ZrP nanosheets have been widely used in gas barrier [13] and flame retardancy [14]. Previously, solution recasting with ZrP nanosheets [11] and swelling incorporation of α-ZrP by in-situ sol-gel process [15–17] have been reported to suppress the permeation of methanol or vanadium ion through Nafion membrane. It is satisfactory to arrange ZrP nanosheets in the vertical direction to the permeation path of vanadium ion so that it can maximize the barrier property of the composite membranes.

Utilizing the ZrP nanosheets with strong negative surface charge, the electrostatic LbL deposition as a promising arrangement route can be taken into account. The LbL assembly represents a simple, efficient, and highly versatile method, which allows the integration of various materials and meets the demand of creating a diverse set of novel highly-ordered nanoarchitectures for extensive practical applications [18]. There has been reported that PDDA/poly(sodium styrene sulfonate) [6,19], poly (allylamine hydrochloride)/PSS [20,21], chitosan/phosphotungstic acid [22,23], 1, 4-phenyldiamine hydrochloride/graphene oxide [24], polyethylenimine/Nafion [25] were built up on the surfaces of IEMs in order to increase the performance of VRFB or direct methanol fuel cell (DMFC). Furthermore, by sequential deposing the charged substrate into oppositely charged electrolyte and inorganic nanosheets, it can fabricate artificial nacre-like structure that mimics the natural LbL approach [26–28].

In this study, Nafion membranes have been first modified by alternative LbL deposition of PDDA and ZrP nanosheets which used as oppositely charged electrolytes. The LbL self-assembled nacre-like nanostructure can function as an effective vanadium-ion-blocking multilayer of Nafion membrane. The morphology of composite membranes were characterized by both SEM and AFM techniques. The dependences of vanadium ion permeabilities and proton conductivities of Nafion-$[PDDA/ZrP]_n$ composite membranes on the number of PDDA/ZrP self-assembled bilayers were further investigated. Finally, VRFB performances of the composite membranes were fully studied and compared with pristine Nafion. The experimental results showed that the VRFB with Nafion-$[PDDA/ZrP]_3$ membrane showed higher CE and EE than VRFB with pristine Nafion membrane.

2. Experimental

2.1. Materials

PDDA (20 wt% in water, Mw = 100 000–200 000, Aladdin), zirconium oxychloride ($ZrOCl_2 \cdot 8H_2O$, 98%, Aladdin), phosphoric acid (H_3PO_4, 85%, Aladdin) and tetrabutylammonium hydroxide (TBAOH, 10 wt%, J&K Scientific Ltd) were used as received. Nafion 115 membrane was purchased from DuPont. Prior to modification, Nafion 115 membrane was treated according to the reported procedure, which was immersed in 3 wt% H_2O_2 solution for 30 min at 80 °C, followed by rinsing with deionized water 5 times, and then in 1 mol L^{-1} H_2SO_4 solution for 2 h at 80 °C, finally stored in deionized water before use. A glass slide (used for SEM examination) was cleaned by immersion in piranha solution (3/1 by v/v of H_2SO_4/H_2O_2) for 1 h, then thoroughly rinsed with deionized water prior to use. This procedure can make the surface of glass slide get charged [27].

2.2. Preparation of ZrP nanosheets suspension

α-ZrP was synthesized according to the previously described process [12,14,29]. A sample of 6.0 g of $ZrOCl_2 \cdot 8H_2O$ was mixed with 60.0 mL of 6.0 mol L^{-1} H_3PO_4 in hydrothermal reaction autoclave and then the autoclave was placed in an oven at 200 °C for 24 h. After the reaction, the raw product was centrifuged and washed with water until the pH of the supernatant reached 5–6. The final α-ZrP was obtained after dried in an oven at 65 °C for 24 h. Then, the prepared α-ZrP (0.10 g in 6.7 mL of water) was exfoliated by TBAOH (3.3 mL of 0.10 mol L^{-1} aqueous solution) and subjected to ultrasonication for 3 h in an ice bath.

2.3. Layer-by-Layer deposition

The LbL self-assembly of the PDDA/ZrP multilayers was carried out by alternately immersing the pretreated Nafion 115 membrane in a PDDA polycation aqueous solution (10 mmol/L) and an aqueous ZrP nanosheets suspension (10 mmol/L) for each 5 min at room temperature. After each immersing step, the membrane was rinsed with deionized water to remove the weakly bonded PDDA and ZrP nanosheets on the membrane surface. The process of alternately dipping in PDDA solution and ZrP nanosheets suspension was then repeated to increase the number of bilayers. The resulting multilayers modified composite membrane was denoted as Nafion-$[PDDA/ZrP]_n$ (n is the number of bilayers), which were stored in deionized water before used. In order to examine the morphologies of the fabricated PDDA/ZrP multilayers, PDDA/ZrP multilayers were also deposited onto glass slide by a same fabrication process.

2.4. Characterization

2.4.1. Instrumentation

The surface morphology of α-ZrP and the cross-section of deposited multilayers were recorded on a scanning electron microscopy (SEM) (Quanta 400, FEI, Netherlands) operated at 15 kV. To investigate the morphology of deposited multilayers, small pieces were cut out of the center of the glass slide with PDDA/ZrP multilayers by a diamond blade and glued on cross-section holders.

The TEM image of ZrP nanosheets was taken on a transmission electron microscopy (Tecnai™ G2 Spirit, FEI, USA) operating at 100 kV.

The surface roughness and morphology of the composite membranes were measured, in air, by CSPM 5500 Atomic Force Microscopy (AFM) operating in the tapping mode.

X-ray diffraction (XRD) patterns were recorded by Bruker D8 Advance X-ray diffractometer using a nickel-filtered Cu-Kα, λ = 1.5406 Å at 40 kV and 30 mA and at a scan rate of 5°/min.

The thermal property of α-ZrP was tested by thermal gravimetric analyzer (TGA, Perkin Elmer Pyris Diamond TG/DTA analyzer) at a heating rate of 10 °C min^{-1} under air atmosphere.

Attenuated total refraction-Fourier transform infrared (ATR-FTIR) spectra were recorded by a Nicolet 6700 FT-IR spectrometer equipped with a temperature-adjustable ATR (Golden Gate) unit and purged with dry air to confirm the successful deposition of PDDA on the surface of the Nafion membrane.

2.4.2. Water uptake (WU) and swelling ratio (SR)

The water uptakes and swelling ratios of the membranes were all measured by comparing the weight changes and volume expansion between dry and hydrated membranes. Prior to the test, the membrane was dried at 80 °C under vacuum for 24 h and its weight, thickness, length and width were measured. Then, the dry membrane was immersed in deionized water at room temperature for 24 h, and the weight, thickness, length and width of the wet membranes were measured after removing the surface water by absorbent paper immediately. The water uptake was defined as the ratio of weight changes of the dry and wet membranes. The swelling ratio, defined in this work, was the volume expansion rate of the wet membrane based on the dry one. They were determined according the following equations:

$$\text{Water uptake } (\%) = \frac{W_w - W_d}{W_w} \times 100\% \quad (1)$$

$$\text{Swelling ratio } (\%) = \frac{X_w \times Y_w \times Z_w - X_d \times Y_d \times Z_d}{X_d \times Y_d \times Z_d} \times 100\% \quad (2)$$

where W_w and W_d represent the weights of membranes before and after water absorption, respectively; X_w and X_d, Y_w and Y_d, Z_w and Z_d are the lengths, widths and thicknesses of the wet and dry membranes, respectively.

2.4.3. Proton conductivity

The proton conductivity of the membranes (effective area S of 0.785 cm^2) was determined by the two-electrode AC impedance spectroscopy method over the frequency range 1 Hz–100 kHz using a Solartron 1255B frequency response analyzer coupled with a Solartron 1287 electrochemical interface at room temperature and 100% relative humidity. The proton conductivity σ is calculated by:

$$\sigma = \frac{d}{RS} \quad (3)$$

where S and d are the effective area and thickness of the membranes.

2.4.4. VO^{2+} permeability

The permeability of VO^{2+} was measured at room temperature by the method according to the literature [30,31]. The membrane (effective area A of 5.3 cm^2) was sandwiched between two diffusion half cells. The left reservoir was filled with 40 mL of 1.5 mol L^{-1} $VOSO_4$ in 3 mol L^{-1} H_2SO_4 solution and the right one was filled with 40 mL of 1.5 mol L^{-1} $MgSO_4$ in 3 mol L^{-1} H_2SO_4 solution. $MgSO_4$ was used to equalize the osmotic pressure. The two solutions were continuously stirred to avoid the concentration polarization. The concentration of VO^{2+} in the right reservoir was monitored by a UV–Vis spectrophotometer (Model: 752-P, Shanghai Xianke Co., China). The VO^{2+} permeability was determined by Fick's diffusion law as the following equation:

$$P = \frac{V_B d}{A(C_A - C_B(t))} \cdot \frac{dC_B(t)}{dt} \quad (4)$$

where P is the permeability of VO^{2+}, V_B is the volume of $MgSO_4$ solution, d and A are the thickness and effective area of the membrane, C_A is VO^{2+} concentration of $VOSO_4$ solution, and $C_B(t)$ is the VO^{2+} concentration of $MgSO_4$ solution as a function of time.

2.4.5. Single VRFB test

A vanadium flow battery was assembled by sandwiching a membrane between two carbon felt electrodes, clamped by two graphite plates according to references [32–34]. The active area of the electrodes is 2 × 3 cm^2. All of these components were fixed between two stainless steel plates. Solutions consisting of 20 mL 1.5 mol L^{-1} VO^{2+}/VO_2^+ in 3.0 mol L^{-1} H_2SO_4 and 20 mL 1.5 mol L^{-1} V^{2+}/V^{3+} in 3.0 mol L^{-1} H_2SO_4 were used as positive and negative electrolytes, respectively. They were cycled with peristaltic pumps. To avoid the corrosion of graphite plates, the upper limit of charge voltage was set at 1.65 V and the lower limit of discharge voltage was set at 0.8 V. Coulombic efficiency (CE), voltage efficiency (VE) and energy efficiency (EE) of VRFB applications are calculated by following equations:

$$CE = \frac{\int I_d dt}{\int I_c dt} \times 100\% \quad (5)$$

$$EE = \frac{\int V_d I_d dt}{\int V_c I_c dt} \times 100\% \quad (6)$$

$$VE = \frac{EE}{CE} \times 100\% \quad (7)$$

where I_c and I_d represent the charge current and discharge current, and V_c and V_d are the charge voltage and discharge voltage, respectively.

A self-discharge test was conducted to further investigate the transfer behavior of vanadium ions across the membranes. In this test, 20 mL 1.5 mol L^{-1} V^{2+}/V^{3+} in 3 mol L^{-1} H_2SO_4 solution and 20 mL 1.5 mol L^{-1} VO^{2+}/VO_2^+ in 3 mol L^{-1} H_2SO_4 solution were cyclically pumped into negative and positive half cells, respectively. Self-discharge started at a state of charge (SOC) of 50%. The procedure was stopped when the open circuit voltage (OCV) was lower than 0.8 V.

3. Results and discussion

3.1. Characterization of α-ZrP and ZrP nanosheets

The thermal characteristic of ZrP was studied by TGA, and the result is displayed in Fig. S1. There are two major weight losses in 100–200 and 450–600 °C ranges. The first weight loss associates with the loss of absorbed water and hydration water, and the

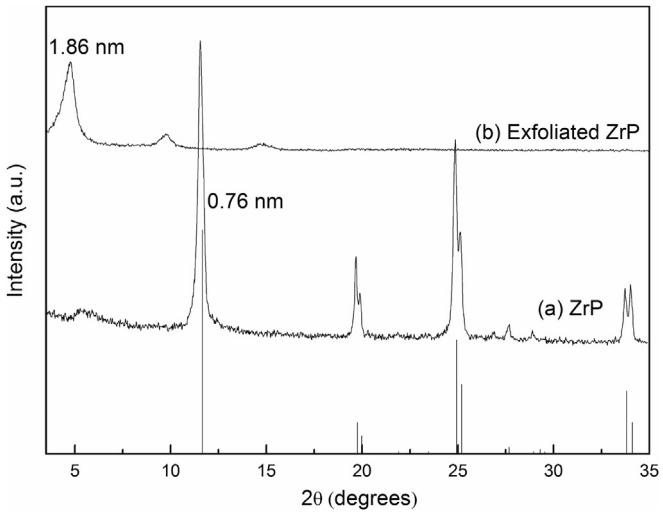

Fig. 1. XRD patterns of α-ZrP and exfoliated ZrP nanosheets.

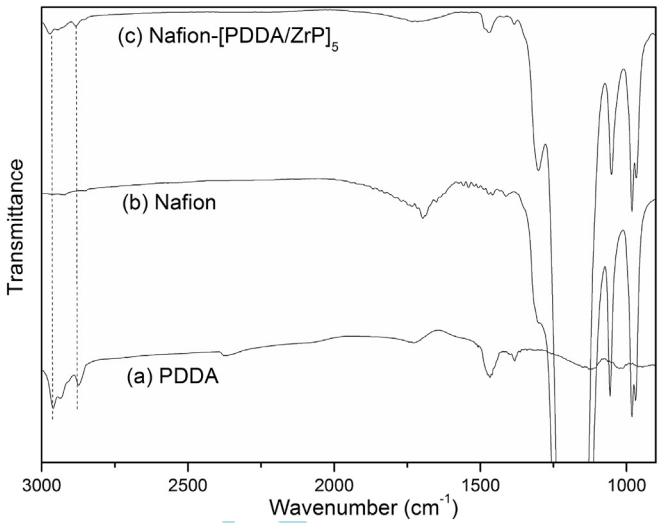

Fig. 3. ATR-FTIR spectra of (a) PDDA, (b) Nafion and (c) Nafion-$[PDDA/ZrP]_5$ membranes.

second weight loss is caused by the condensation water in α-ZrP [29]. The FTIR spectrum (Fig. S2) of the α-ZrP demonstrates the presence of −OH from lamellar surface stretching and bending vibration at 3165 and 1620 cm^{-1}, P-OH in-plane and out-of-plane vibration at 970 and 1251 cm^{-1}. The bands at 1047 and 1121 cm^{-1} are attributed to O-P-O stretching vibrations which are the major bands in the spectrum. Respectively, the Zr−O stretching vibration lies at 534 and 593 cm^{-1}.

Fig. 1 presents the XRD patterns of α-ZrP and the exfoliated ZrP nanosheets. α-ZrP was tested in a powder form, while the exfoliated ZrP nanosheets were dried on a silicon wafer for XRD characterization. The XRD patterns clearly show that the strong peak at 11.7° (0.76 nm) is the lamellas distance of α-ZrP, and the small peak at 4.7° (1.86 nm) is due to exfoliated ZrP nanosheets restacking an ordered layered structure after drying. The results reveal that α-ZrP can be directly intercalated and exfoliated by TBAOH in aqueous solution at low temperatures.

Both SEM and TEM techniques are used to observe the morphologies of α-ZrP and the exfoliated ZrP. Fig. 2(a) displays the SEM micrograph of α-ZrP. The regular hexagonal structure means the high degree of crystallinity of α-ZrP. The TEM image (Fig. 2(b)) of the exfoliated ZrP shows that ZrP nanosheets can be completely exfoliated by TBAOH in aqueous solution, appearing flake-like morphology with some unique wrinkles according to the reported literature [29,35].

3.2. Characterization of Nafion-$[PDDA/ZrP]_n$ membranes

According to the literature [20,22,23], UV-vis spectroscopy is generally used to verify the presence of the deposited multilayers of LbL self-assembly. However, ZrP nanosheets and PDDA are almost transparent in the UV-vis spectral range. In this sense, to confirm the appearance of the Nafion surface covered with PDDA, ATR-FTIR spectra were recorded of pure PDDA, unmodified Nafion and Nafion-$[PDDA/ZrP]_5$ membrane in turn. It can be seen in Fig. 3 that a doublet band (2938 cm^{-1}, 2865 cm^{-1}) in the 2800–2900 cm^{-1} region due to the stretching vibration of the methyl group. This indicates that PDDA has been successfully deposited on the surface of the Nafion membrane.

In Fig. 4, a layered structure can be observed by cross-section SEM image of $[PDDA/ZrP]_{15}$ film, which is conceptually similar to that of nacre. The self-assembled multilayers are about 150 nm in the thickness of fifteen PDDA/ZrP bilayers. It can be calculated that thickness of each PDDA/ZrP bilayer approximates 10 nm, which is thicker than the theoretical value. This is not accurately in

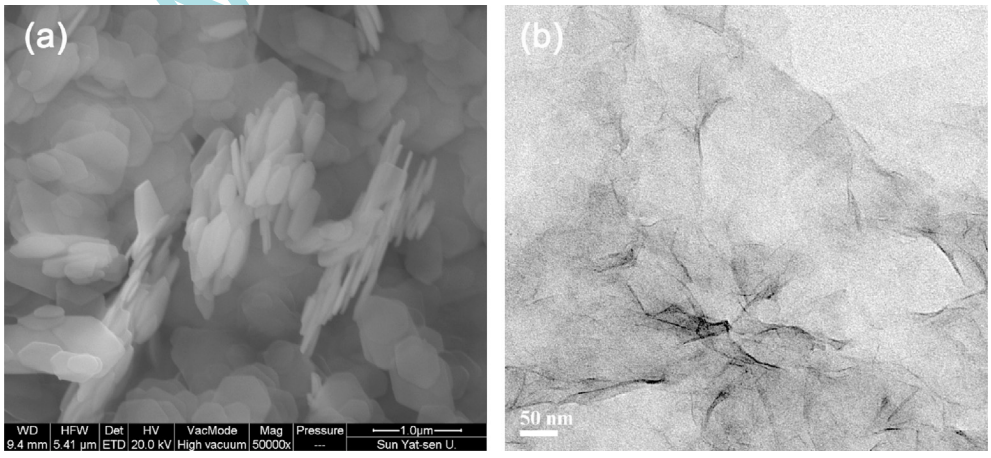

Fig. 2. (a) SEM image of α-ZrP; (b) TEM image of the exfoliated ZrP nanosheets.

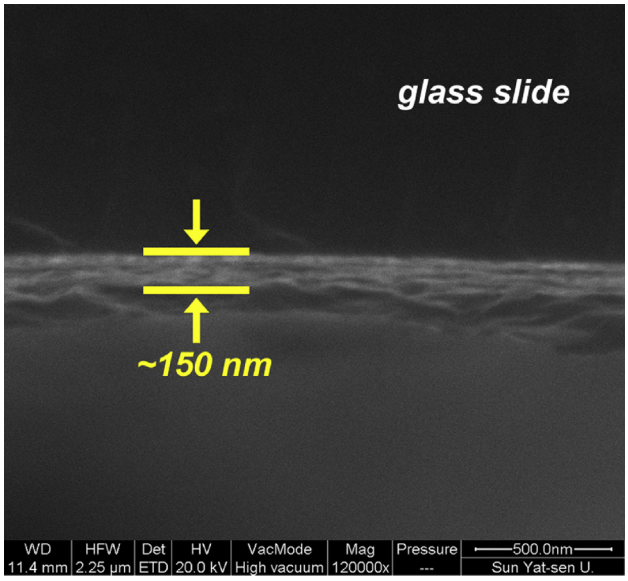

Fig. 4. SEM cross-sectional view of $[PDDA/ZrP]_{15}$ multilayers.

agreement with the LbL repeated deposition cycles. Presumably, it is because the wrinkles and aggregates of ZrP nanosheets increase the thickness of the bilayer. Moreover, the morphology and topography of pristine Nafion and Nafion-$[PDDA/ZrP]_3$ membrane were further measured by AFM. The successfully deposition of PDDA/ZrP bilayers are verified by AFM micrographs (Fig. 5). The roughness of the Nafion membrane surface apparently increases after self-assembled.

3.3. Water uptake and swelling ratio

The physicochemical properties, such as water uptake and swelling ratio of pristine Nafion and Nafion-$[PDDA/ZrP]_n$ membrane were measured and the results are shown in Fig. 6(a). The water uptake and swelling ratio of the Nafion-$[PDDA/ZrP]_n$ membrane decrease slightly with increasing the number of PDDA/ZrP bilayers. It means that the LbL self-assembly of PDDA/ZrP can effectively suppress the hydrophilicity of Nafion.

3.4. Proton conductivity, vanadium ion permeability and ion selectivity

The proton conductivity and vanadium ion permeability of the membranes were determined and the results were presented in Fig. 6(b) and (c). The proton conductivities of Nafion-$[PDDA/ZrP]_n$ membranes are lower than that of pristine Nafion and slightly decreased with increasing the number of self-assembled bilayers. It is believed that ZrP nanosheets barrier layers generate more tortuous diffusion paths and prohibit the proton transportation, despite ZrP nanosheets are one of the fastest proton conductors with high IEC (6.64 meq g^{-1}) [36].

It has been reported that the diffusion coefficients of vanadium ions cross Nafion 115 are in the order of $V^{2+}>VO^{2+}>VO_2^+>V^{3+}$ in the permeability test [37]. According to this result, VO^{2+} ion exhibits a much faster crossover compared with VO^{2+} or V^{3+}. Therefore, only did the permeation behavior of VO^{2+} ion is determined. Meanwhile, Given V^{2+} is too active in air to be measured [38]. Consequently, VO^{2+} permeating test is generally performed to evaluate the penetration of vanadium ions, other than the species of V^{2+}, V^{3+}, VO^{2+} and VO^{2+} [39]. It is generally known that high vanadium ion permeability is the fatal weakness of Nafion membrane generating rapid self-discharge of the VRFB, and resulting in low energy efficiency. As shown in Fig. 6(b), during the test process, the vanadium ion concentration permeating across the Nafion-$[PDDA/ZrP]_n$ membranes is lower than that of pristine Nafion. As to the large size of vanadium ion, its permeability decreases dramatically compared with proton conductivity, with increasing the number of self-assembled bilayers. After deposited only one PDDA/ZrP bilayer, the vanadium ion permeability of Nafion reduces 50%. Particularly, the composite membrane with four bilayers shows two orders of magnitude lower vanadium ion permeability (1.05×10^{-6} cm^2 min^{-1}) than that of pristine Nafion (1.54×10^{-8} cm^2 min^{-1}) at room temperature. It can be explained that the introduction of PDDA with positive charges could suppress the vanadium ions via Donnan exclusion effect. Meanwhile, the lamellar structure of ZrP nanosheets effectively serves as barriers to prevent vanadium ions migrating through the membrane.

Generally, as a comprehensive parameter for evaluating the membrane performance, ion selectivity of proton conductivity is defined as the ratio of proton conductivity to vanadium ion permeability. A higher ion selectivity value promises better performance in VRFB applications [40]. Fig. 6(d) illustrates that the ion selectivity of the composite membrane increases with increasing the number of PDDA/ZrP bilayers. It might be due to the smaller stoke radius of proton compared with vanadium ions and leading to more easily proton transporting across the membrane. Moreover, the ion selectivity of the Nafion-$[PDDA/ZrP]_4$ membrane is 12 times higher than that of pristine Nafion. In order to compare this work with previously reported ones, some relevant literature are listed in Table S1. Because of different modification methods of Nafion-based membranes and various characterization techniques, the specific data from different literature could only be a reference.

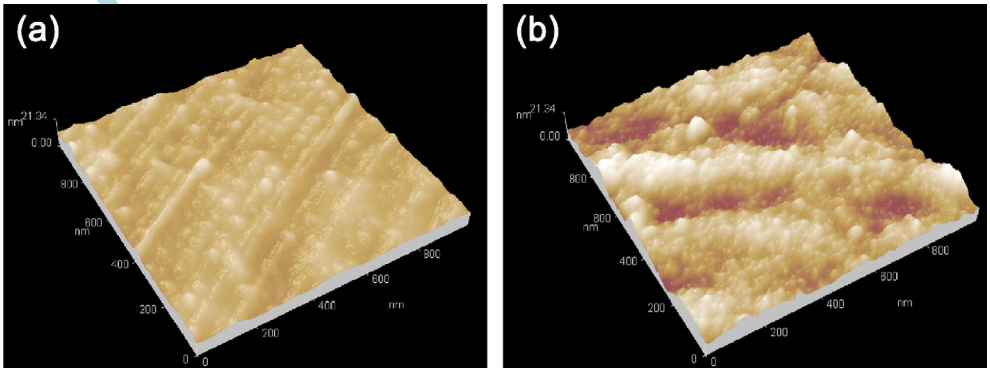

Fig. 5. AFM micrographs of (a) Nafion and (b) Nafion-$[PDDA/ZrP]_3$ membranes.

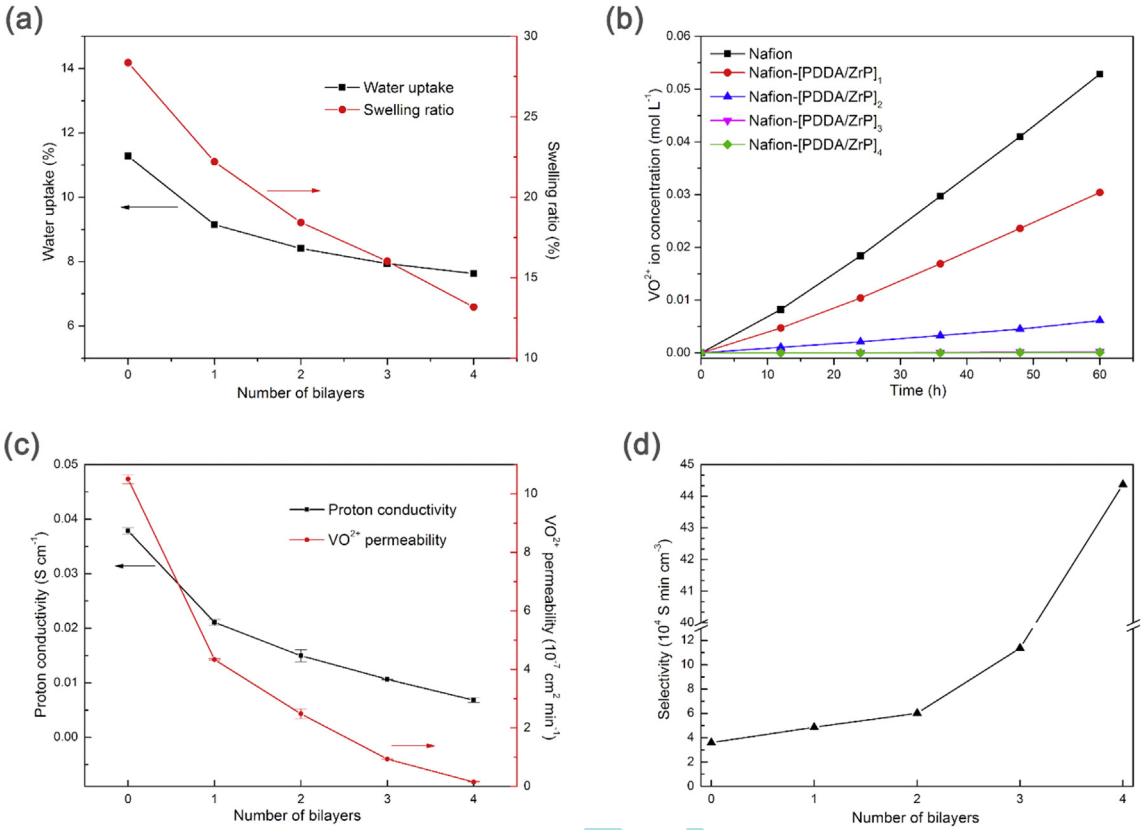

Fig. 6. The characterization of Nafion-[PDDA/ZrP]$_n$ membranes as function of the number of PDDA/ZrP bilayers: (a) Water uptake and swelling ratio; (b) VO^{2+} ion concentration versus time at the diffusion side; (c) Proton conductivity and vanadium ion permeability; (d) Ion selectivity.

Clearly, the Nafion-[PDDA/ZrP]$_3$ membrane shows 3 times higher ion selectivity than that of pristine Nafion membrane. The result is much better than others. According to the above, the composite Nafion membranes can dramatically suppress the vanadium ions permeability, demonstrating their great potential for future application in VRFB.

3.5. Battery performance of VRFBs

Considering the comprehensive performances of proton conductivity, vanadium ion permeability and ion selectivity, Nafion-[PDDA/ZrP]$_3$ membrane was chosen to VRFB evaluation. Fig. S3 displays the charge-discharge curves of VRFBs with pristine Nafion and Nafion-[PDDA/ZrP]$_3$ membrane at different current densities. The comparisons of CE, VE and EE are presented in Fig. 7. Owing to the reduced time for concentration-gradient-driven vanadium ion cross-over at higher current densities, the battery CE increases with increasing current density. On the contrary, the battery VE decreases due to larger internal losses [8].

The results indicate that the charge–discharge capacity of the VRFB with Nafion-[PDDA/ZrP]$_3$ membrane exhibits higher CE and EE than those of pristine Nafion VRFB at the current density ranging from 10 to 50 mA cm^{-2}. The enhanced CE is attributed to less cross-over of vanadium ions. Although there is small reduced of VE due to the proton conductivity slightly sacrificed, Nafion-[PDDA/ZrP]$_3$ membrane shows higher EE than pristine Nafion at the current density, which implies that the Nafion-[PDDA/ZrP]$_3$ membrane has higher energy conversion efficiency in large-scale energy storage devices.

Vanadium ion permeation generally results in self-discharge, and the self-discharge degree of VRFB is typically evaluated by monitoring the change of OCV value. The VRFBs self-discharge with pristine Nafion and Nafion-[PDDA/ZrP]$_3$ membrane were characterized by monitoring the OCV started at the state of charge (SOC) of 50%. Fig. 8 shows that the OCV values decrease gradually and exhibit an almost linear relationship with storage time and then drop sharply to 0.8 V. The timings of the voltage remaining above 0.8 V are 31 h and 42 h for pristine Nafion and Nafion-[PDDA/ZrP]$_3$ membrane, respectively. The OCV decay rate for Nafion-[PDDA/

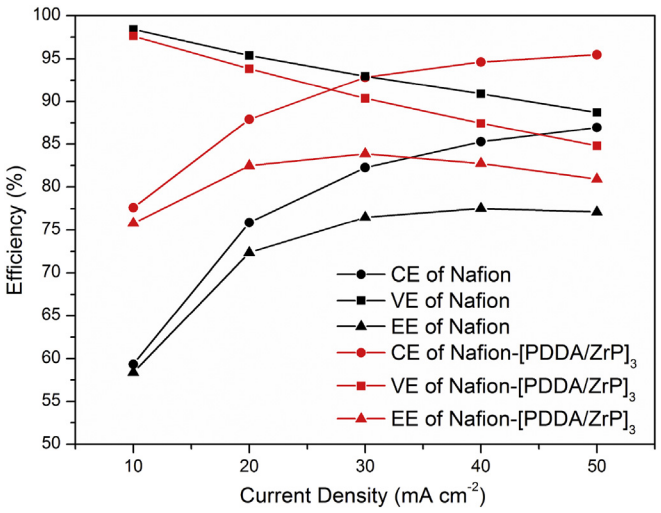

Fig. 7. Comparison of efficiency between the VRFBs equipped with Nafion and Nafion-[PDDA/ZrP]$_3$ membranes.

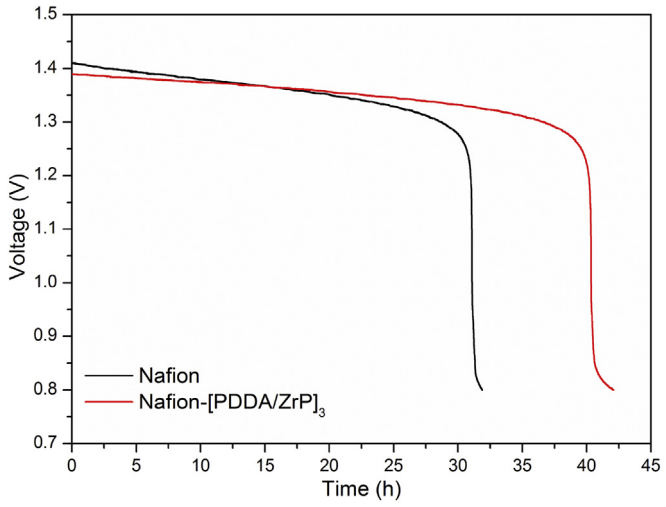

Fig. 8. Open circuit voltage (OCV) of VRFBs with Nafion and Nafion-[PDDA/ZrP]$_3$ membranes as a function of time at the state of charge (SOC) of 50%, respectively.

ZrP]$_3$ membrane is much slower than that of pristine Nafion. It is in accordance well with the changing trends of VO^{2+} permeability and ion selectivity, indicating that the Nafion-[PDDA/ZrP]$_3$ membrane exhibits longer charge retention time and an excellent performance for VRFB application.

4. Conclusions

The nacre-like nanostructured composite membranes can be prepared by the self-assembly of PDDA/ZrP bilayers on the surface of Nafion membrane, and successfully used in VRFB applications. The PDDA and well-organized ZrP nanosheets on the surface of Nafion act as electrostatic repulsion and physical barrier, respectively, to suppress vanadium ions from cross-mixing, resulting in much lower vanadium ion permeability and higher ion selectivity of the composite membrane. The as-prepared Nafion-[PDDA/ZrP]$_4$ membrane shows two orders of magnitude lower vanadium ion permeability (1.05×10^{-6} cm^2 min^{-1}) and 12 times higher ion selectivity than those of pristine Nafion membrane at room temperature. Consequently, the performance of the VRFBs assembled with Nafion-[PDDA/ZrP]$_3$ membrane demonstrated a highly CE and EE together with a very slow self-discharge rate. When comparing with pristine Nafion VRFB, the CE and EE values of Nafion-[PDDA/ZrP]$_3$ VRFB are 10% and 7% higher at 30 mA cm^{-2}, respectively.

Acknowledgments

The authors would like to thank the Link Project of the National Natural Science Foundation of China and Guangdong Province (Grant No. U1601211); National Natural Science Foundation of China (Grant No. 51573215, 21506260); Guangdong Province Sci & Tech Bureau Key Strategic Project (Grant No. 2016B010114004), Natural Science Foundation of Guangdong Province (Grant No. 2014A030313159, 2016A030313354), the Special Project on the Integration of Industry, Education and Research of Guangdong Province (Grant No. 2015B090901001, 2014B090904064, 2013B090500004), Guangzhou Scientific and Technological Planning Project (2014J4500002, 201607010042) for financial support of this work.

Appendix A. Supplementary data

Supplementary data related to this article can be found at http://dx.doi.org/10.1016/j.jpowsour.2017.03.124.

References

[1] M. Ulaganathan, V. Aravindan, Q. Yan, S. Madhavi, M. Skyllas-Kazacos, T.M. Lim, Adv. Mater. Interfaces 3 (2016) 1–22.
[2] S.-H. Cha, J. Nanomater. 2015 (2015) 1–12.
[3] T.N.L. Doan, T.K.A. Hoang, P. Chen, RSC Adv. 5 (2015) 72805–72815.
[4] L. Joerissen, J. Garche, C. Fabjan, G. Tomazic, J. Power Sources 127 (2004) 98–104.
[5] C. Ponce de León, A. Frías-Ferrer, J. González-García, D.A. Szánto, F.C. Walsh, J. Power Sources 160 (2006) 716–732.
[6] J.Y. Xi, Z.H. Wu, X.G. Teng, Y.T. Zhao, L.Q. Chen, X.P. Qiu, J. Mater. Chem. 18 (2008) 1232–1238.
[7] E.M. Davis, J. Kim, V.P. Oleshko, K.A. Page, C.L. Soles, Adv. Funct. Mater. 25 (2015) 4064–4075.
[8] R.D. Yang, Z.S. Cao, S.W. Yang, I. Michos, Z. Xu, J.H. Dong, J. Membr. Sci. 484 (2015) 1–9.
[9] X.G. Teng, J.C. Dai, J. Su, Y.M. Zhu, H.P. Liu, Z.G. Song, J. Power Sources 240 (2013) 131–139.
[10] C.-H. Lin, M.-C. Yang, H.-J. Wei, J. Power Sources 282 (2015) 562–571.
[11] Y. Kozawa, S. Suzuki, M. Miyayama, T. Okumiya, E. Traversa, Solid State Ionics 181 (2010) 348–353.
[12] W.J.B. Luyi Sun, Dazhi Sun, Abraham Clearfield, Hung-Jue Sue, Chem. Mater. 19 (2007) 1749–1754.
[13] M.H. Wong, R. Ishige, K.L. White, P. Li, D. Kim, R. Krishnamoorti, R. Gunther, T. Higuchi, H. Jinnai, A. Takahara, R. Nishimura, H.-J. Sue, Nat. Commun. 5 (2014) 1–12.
[14] Y. Pan, H.F. Pan, B.H. Yuan, N.N. Hong, J. Zhan, B.B. Wang, L. Song, Y. Hu, Mater. Chem. Phys. 163 (2015) 107–115.
[15] M. Casciola, D. Capitani, A. Comite, A. Donnadio, V. Frittella, M. Pica, M. Sganappa, A. Varzi, Fuel Cells 8 (2008) 217–224.
[16] J. Pandey, M.M. Seepana, A. Shukla, Int. J. Hydrogen Energy 40 (2015) 9410–9421.
[17] S.B. Sang, Q.M. Wu, K.L. Huang, J. Membr. Sci. 305 (2007) 118–124.
[18] F.-X. Xiao, M. Pagliaro, Y.-J. Xu, B. Liu, Chem. Soc. Rev. 45 (2016) 3088–3121.
[19] Y.F. Wang, S.J. Wang, M. Xiao, D.M. Han, M.A. Hickner, Y.Z. Meng, RSC Adv. 3 (2013) 15467–15474.
[20] H. Deligöz, S. Yılmaztürk, T. Karaca, H. Özdemir, S.N. Koç, F. Öksüzömer, A. Durmuş, M.A. Gürkaynak, J. Membr. Sci. 326 (2009) 643–649.
[21] S. Yılmaztürk, H. Deligöz, M. Yılmazoğlu, H. Damyan, F. Öksüzömer, S.N. Koç, A. Durmuş, M.A. Gürkaynak, J. Membr. Sci. 343 (2009) 137–146.
[22] C.J. Zhao, H.D. Lin, Z.M. Cui, X.F. Li, H. Na, W. Xing, J. Power Sources 194 (2009) 168–174.
[23] S.F. Lu, C.X. Wu, D.W. Liang, Q.L. Tan, Y. Xiang, RSC Adv. 4 (2014) 24831–24837.
[24] L.S. Wang, A.N. Lai, C.X. Lin, Q.G. Zhang, A.M. Zhu, Q.L. Liu, J. Membr. Sci. 492 (2015) 58–66.
[25] G.J. Austing, N.C. Kirchner, L. Komsiyska, G. Wittstock, J. Membr. Sci. 510 (2016) 259–269.
[26] Z.Y. Tang, N.A. Kotov, S. Magonov, B. Ozturk, Nat. Mater. 2 (2003) 413–418.
[27] P. Podsiadlo, S. Paternel, J.-M. Rouillard, Z.F. Zhang, J. Lee, J.-W. Lee, E. Gulari, N.A. Kotov, Langmuir 21 (2005) 11915–11921.
[28] S.M. Waraich, B. Hering, Z. Burghard, J. Bill, P. Behrens, H. Menzel, J. Colloid Interface Sci. 367 (2012) 74–82.
[29] Y.J. Zhou, R.C. Huang, F.C. Ding, A.D. Brittain, J.J. Liu, M. Zhang, M. Xiao, Y.Z. Meng, L.Y. Sun, ACS Appl. Mater. Interfaces 6 (2014) 7417–7425.
[30] D. Chen, S. Wang, M. Xiao, D. Han, Y. Meng, J. Power Sources 195 (2010) 7701–7708.
[31] D. Chen, S. Wang, M. Xiao, Y. Meng, J. Power Sources 195 (2010) 2089–2095.
[32] Z.Z. Yuan, X.X. Zhu, M.R. Li, W.J. Lu, X.F. Li, H.M. Zhang, Angew. Chem. Int. Ed. 55 (2016) 3058–3062.
[33] J. Pan, S. Wang, M. Xiao, M. Hickner, Y. Meng, J. Membr. Sci. 443 (2013) 19–27.
[34] D. Chen, S. Wang, M. Xiao, Y. Meng, Energy Environ. Sci. 3 (2010) 622–628.
[35] L.Y. Sun, W.J. Boo, R.L. Browning, H.-J. Sue, A. Clearfield, Chem. Mater. 17 (2005) 5606–5609.
[36] A. Clearfield, Chem. Rev. 88 (1988) 125–148.
[37] C. Sun, J. Chen, H. Zhang, X. Han, Q. Luo, J. Power Sources 195 (2010) 890–897.
[38] K. Ngamsai, A. Arpornwichanop, J. Power Sources 295 (2015) 292–298.
[39] J.B. Liao, M.Z. Lu, Y.Q. Chu, J.L. Wang, J. Power Sources 282 (2015) 241–247.
[40] J. Shen, J.Y. Xi, W.T. Zhu, L.Q. Chen, X.P. Qiu, J. Power Sources 159 (2006) 894–899.